

HEMATOPOIESIS AND STEM CELLS

Genome-wide association study on 13 167 individuals identifies regulators of blood CD34⁺ cell levels

Aitzkoa Lopez de Lapuente Portilla,^{1,2} Ludvig Ekdahl,^{1,2,*} Caterina Cafaro,^{1,2,*} Zain Ali,^{1,2,*} Natsumi Miharada,^{1,2} Gudmar Thorleifsson,³ Kristijonas Žemaitis,^{1,2} Antton Lamarca Arrizabalaga,^{1,2} Malte Thodberg,^{1,2} Maroulio Pertesi,^{1,2} Parashar Dhapola,^{1,2} Erik Bao,⁴⁻⁶ Abhishek Niroula,^{1,2,6} Divya Bali,^{1,2} Gudmundur Norddahl,³ Nerea Ugidos Damboriena,^{1,2} Vijay G. Sankaran,⁴⁻⁶ Göran Karlsson,^{1,2} Unnr Thorsteinsdottir,³ Jonas Larsson,^{1,2} Kari Stefansson,³ and Björn Nilsson^{1,2,6}

¹Lund Stem Cell Center; ²Department of Laboratory Medicine, Lund University, Lund, Sweden; ³deCODE genetics/Amgen Inc., Reykjavik, Iceland; ⁴Division of Hematology and Oncology, Boston Children's Hospital and Department of Pediatric Oncology, Dana-Farber Cancer Institute, Harvard Medical School, Boston, MA; ⁵Harvard Stem Cell Institute, Cambridge, MA; and ⁶Broad Institute, Cambridge, MA

KEY POINTS

- We report a large-scale genome-wide association study on blood CD34⁺ cell levels, identifying 9 significant and 2 suggestive variants.
- The most significant associations map to *CXCR4* and *PPM1H*, the latter a potential inhibition target for stem cell mobilization.

Stem cell transplantation is a cornerstone in the treatment of blood malignancies. The most common method to harvest stem cells for transplantation is by leukapheresis, requiring mobilization of CD34⁺ hematopoietic stem and progenitor cells (HSPCs) from the bone marrow into the blood. Identifying the genetic factors that control blood CD34⁺ cell levels could reveal new drug targets for HSPC mobilization. Here we report the first large-scale, genome-wide association study on blood CD34⁺ cell levels. Across 13 167 individuals, we identify 9 significant and 2 suggestive associations, accounted for by 8 loci (*PPM1H*, *CXCR4*, *ENO1-RERE*, *ITGA9*, *ARHGAP45*, *CEBPA*, *TERT*, and *MYC*). Notably, 4 of the identified associations map to *CXCR4*, showing that bona fide regulators of blood CD34⁺ cell levels can be identified through genetic variation. Further, the most significant association maps to *PPM1H*, encoding a serine/threonine phosphatase never previously implicated in HSPC biology. *PPM1H* is expressed in HSPCs, and the allele that confers higher blood CD34⁺ cell levels downregulates *PPM1H*. Through functional fine-mapping, we find that this downregulation is caused by the variant rs772557-A, which abrogates an MYB transcription

factor-binding site in *PPM1H* intron 1 that is active in specific HSPC subpopulations, including hematopoietic stem cells, and interacts with the promoter by chromatin looping. Furthermore, *PPM1H* knockdown increases the proportion of CD34⁺ and CD34⁺90⁺ cells in cord blood assays. Our results provide the first large-scale analysis of the genetic architecture of blood CD34⁺ cell levels and warrant further investigation of *PPM1H* as a potential inhibition target for stem cell mobilization.

Introduction

Human hematopoiesis is defined by the outgrowth of mature blood cells through successive proliferation and differentiation of hematopoietic stem and progenitor cells (HSPCs).¹ In blood, HSPCs constitute a tiny (~0.1%) subset of mononuclear white blood cells. Circulating HSPCs express the surface protein CD34, allowing quantification by flow cytometry.² Epidemiologic studies^{3,4} indicate that blood CD34⁺ cell levels are partly genetically determined. However, the underlying DNA sequence variants and genes remain unknown, and no genome-wide significant associations have been reported.³

To identify DNA sequence variants that influence blood CD34⁺ cell levels, we conducted a genome-wide association study (GWAS). We identified 9 significant and 2 suggestive association signals, including 4 independent associations with *CXCR4* and an association with *PPM1H*. Notably, *PPM1H* encodes a serine/

threonine phosphatase previously not implicated in HSPC biology. Relative to other blood cell types, *PPM1H* is preferentially expressed in HSPCs. The allele that confers higher blood CD34⁺ cell levels downregulates *PPM1H* in CD34⁺ cells due to loss of an MYB transcription factor-binding site. Our results provide new insight into the regulation of blood CD34⁺ cell levels and warrant further studies of *PPM1H* as a potential inhibition target to facilitate stem cell mobilization.

Methods

The methods and materials are described in detail in the supplemental Methods (available on the *Blood* Web site).

Sample collection

We collected 16 931 peripheral blood samples from blood donors (n = 7773) and primary care patients (n = 9158) in 3 phases:

November 2015 to April 2016 (Phase I); January 2017 to November 2017 (Phase II); and August 2018 to April 2019 (Phase III) (Lund University Ethical Review Board; dnr 2018/2) (supplemental Table 1; supplemental Figure 1). Information about sex was available for all participants and age for 8251 participants. After quality control, 13 167 unique individuals remained.

Flow cytometry phenotyping

After red blood cell lysis, white blood cells were washed twice, stained with antibody cocktail containing anti-CD45-APC-H7 and either anti-CD34-PerCP-Cy5.5 or anti-CD34-PE-CF594 (supplemental Table 2), and analyzed by using a BD FACS Canto II (Phase I), BD LSR Fortessa (Phase II), or Bio-Rad ZE5 (Phase III) (supplemental Table 3). Samples were processed within 36 hours of blood draw.

Gating of flow cytometry data for association study

To quantify blood CD34⁺ cell levels, we gated singlet peripheral blood mononuclear cells (PBMCs) based on forward scatter area, forward scatter height, and side scatter area, and then CD34⁺45^{low} cells and CD45⁺ cells within PBMCs. The CD34⁺ level was defined as the number of CD34⁺45^{low} cells divided by the number of CD45⁺ PBMCs (supplemental Figure 2).

To facilitate analysis of the large volume of flow cytometry data, we developed pattern recognition software (AliGater; <https://github.com/LudvigEk/AliGater>; gating strategies at <https://github.com/LudvigEk/HSPC-regulators-in-human-blood>) (supplemental Methods; supplemental Figure 3). Phase I and II samples were gated by using AliGater; Phase III samples were gated manually by using FlowJo (FlowJo LLC). Minor differences in CD34⁺ levels were observed between phases (median, 9.11×10^{-4} CD34⁺ per CD45⁺PBMCs in Phase I; 9.66×10^{-4} in Phase II and 1.0×10^{-3} in Phase III; Kruskal-Wallis test, $P = 4.0 \times 10^{-88}$) (supplemental Table 3), likely because of the use of different flow cytometers and antibody panels.

Genotyping and association analysis

Samples were genotyped by using Illumina OmniExpress-24 and Global Screening single-nucleotide polymorphism (SNP) microarrays. For imputation, we used pre-existing whole-genome sequence data for 17 408 individuals of European origin, including 3704 Swedish individuals. Using ancestry analysis, the association data were partitioned into a discovery set of 10 949 individuals of Swedish ancestry and a follow-up set of 2218 individuals of non-Swedish European ancestry. Association testing was performed by using linear regression in the discovery and follow-up sets separately; the results were combined through meta-analysis using a fixed effects inverse variance method.⁵ To adjust for multiple testing, class-based Bonferroni significance thresholds were used.⁶ To identify underlying independent signals, we used step-wise conditional analysis. To define the 99% credible set of plausible causal variants for each association signal, we used a Bayesian refinement approach.⁷

Chromatin accessibility data

To identify candidate causal regulatory variants, we used Assay for Transposase-Accessible Chromatin using sequencing (ATAC-seq) data for sorted blood cell types.^{8,9} To screen for genomic regions that drive candidate gene expression, these data were

integrated with messenger RNA-sequencing (RNA-seq) data for the same cell types, by testing for correlation across blood cell types between gene expression and ATAC-seq signal intensity (averaged across a 100-bp sliding window positioned at every 50 bp). To map chromatin accessibility in MOLM13 cells, ATAC-seq was performed on 50 000 cells¹⁰ (raw sequencing data in Sequence Read Archive, accession number PRJNA761267). To test for allele-dependent accessibility at rs772557, we used publicly available ENCODE DNase-sequencing data for primary adult CD34⁺ cells from a single heterozygous individual.¹¹

Heritability estimation

Total narrow-sense heritability was estimated with the linkage disequilibrium score regression (LDSC) software.^{12,13} To estimate cell type-specific partitioned heritability based on chromatin accessibility, we used LD scores based on ATAC-seq data for sorted blood cell types available for LDSC.¹² This was extended with LD scores for myeloid and plasmacytoid dendritic cells computed by using LDSC from published ATAC-seq data⁸ (National Center for Biotechnology Information Gene Expression Omnibus accession number GSE119453).

Promoter capture Hi-C data analysis

To identify variants that interact with gene promoters, we used published promoter capture Hi-C (PCHi-C) data for CD34⁺ cells (ArrayExpress accession number E-MTAB-2323).¹⁴

Chromatin immunoprecipitation-sequencing data

To test allele-specific binding of MYB to rs772557, we used MYB chromatin immunoprecipitation with massively parallel DNA sequencing data¹⁵ and whole-genome sequencing data¹⁶ for Jurkat cells (Sequence Read Archive accession numbers SRR1603653 and SRR5349449).

Expression quantitative trait locus analysis in blood CD34⁺ cells

We purified CD34⁺ cells from 155 blood donors using immunomagnetic bead enrichment followed by fluorescence-activated cell sorting within 8 hours of blood draw (14 000 to 358 000 cells per sample; average, 122 000). After RNA extraction and complementary DNA synthesis, samples were sequenced on an Illumina NovaSeq 6000 sequencer. To test for associations between variants and gene expression, we used linear modeling with the variant genotype as independent variable and 10 expression principal component covariates. For *CXCR4*, the 3 common variants were included as independent variables in the same model. *P* values were calculated by using Student *t* test for the independent variables. The sequencing data and counts of Fragments Per Kilobase of transcript per Million mapped reads are available from the European Genome Archive repository (accession numbers EGAS00001005655 and EGAD00001008194).

Gene expression data and analysis

To map candidate gene expression, we used single-cell RNA-seq data for 35 582 mononuclear cells from blood and bone marrow,¹⁷ and bulk RNA-seq data for sorted blood cell types.⁸ In addition, we used single-cell Cellular Indexing of Transcriptomes and Epitopes by Sequencing data on 4905 CD34⁺ cells from adult bone marrow.¹⁸ For dimension reduction, we used Uniform Manifold Approximation and Projection¹⁹ and imputed gene expression using MAGIC were used.²⁰

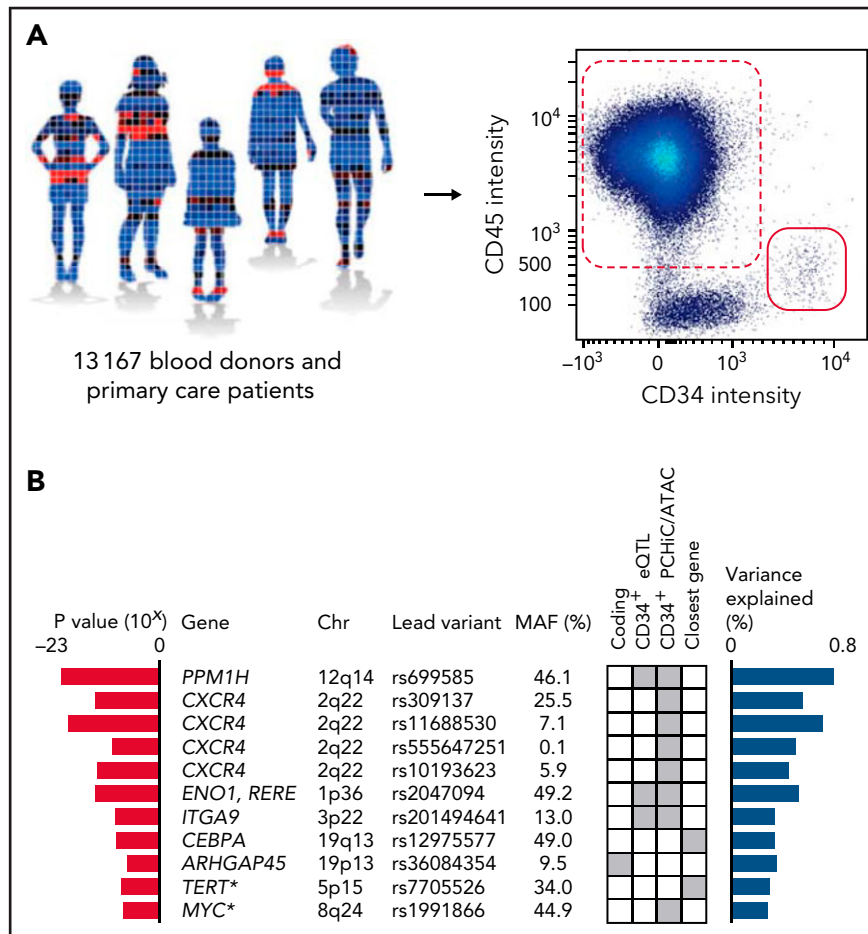


Figure 1. GWAS. (A) A GWAS was performed on blood CD34⁺ cell levels in 13167 individuals, including 10949 of Swedish ancestry and 2218 of non-Swedish European ancestry. The CD34⁺ level was defined as the number of CD34⁺ cells (red solid) divided by the number of CD45⁺ mononuclear cells (red dashed) (supplemental Figure 2). (B) In a combined analysis of the individuals of Swedish ancestry and the individuals of non-Swedish European ancestry, 9 significant and 2 suggestive (asterisks) associations (having *P* values within one order of magnitude from Bonferroni thresholds) were identified (supplemental Tables 5-8). The listed variants are the most significant (lead) variants for each association. Red bars indicate *P* values for association with blood CD34⁺ cell levels for the lead variants in the combined analysis. Blue bars indicate proportion of variance explained. Gene names indicate the likely candidate genes of each association. Genes were prioritized as candidate genes if they: (1) had a coding variant within the 99% credible set of probable causal variants (supplemental Table 9); (2) had a *cis*-eQTL in CD34⁺ cells (supplemental Table 10); or (3) the credible set contained a regulatory variant that maps either to the promoter or to a region with a chromatin looping interaction with the promoter in CD34⁺ cells. If none of these criteria were fulfilled, the closest gene was prioritized. The criterion used to call each gene a candidate gene is indicated by gray squares in the matrix. MAF, minor allele frequency.

CRISPR/Cas9 perturbation of variant regions

We used dual-single guide RNA (sgRNA) CRISPR/Cas9 to delete the regions harboring the 4 candidate causal variants at *CXCR4*, and an allele-specific single-sgRNA CRISPR/Cas9 approach to perturb rs772557 at *PPM1H* (supplemental Table 4). sgRNAs were cloned into the pSpCas9(BB)-2A-GFP PX458 vector and transfected into MOLM13 cells (*CXCR4* variants) or K562 cells (*PPM1H* rs772557 variant). At 24 hours posttransfection, green fluorescent protein-positive cells were isolated by fluorescence-activated cell sorting. Deletion in MOLM13 cells was verified by polymerase chain reaction and electrophoresis in a 1% agarose gel. Deletion efficiency was estimated as the intensity of the deletion band divided by the sum of the intensity of the deletion band and the intensity of the wild-type band. For allele-specific CRISPR/Cas9 toward rs772557 in K562 cells, perturbation was verified by using Sanger sequencing and the Tracking of Indels by Decomposition (TIDE, <https://tide.nki.nl/>). As control, we used sgRNAs targeting a random noncoding region on a different chromosome. *CXCR4* and *PPM1H* expression after

CRISPR/Cas9 perturbation was quantified by using quantitative polymerase chain reaction.

Luciferase experiments

For the *PPM1H* variants, 200-bp sequences representing the reference and alternative allele of rs772555, rs772556, rs772557, and rs772559 in their genomic contexts were synthesized as gBlocks and cloned into the pGL3-Basic plasmid using *KpnI* and *BglIII* restriction sites.

Sequences were centered on the variant, and the 2 constructs differed only for the variant. Renilla luciferase constructs were cotransfected with firefly construct into K562 cells. At 24 hours postelectroporation, luciferase and Renilla activities were measured. Based on the readings, log₂ scores were calculated for each variant reflecting the luciferase activity of the alternative allele relative to the reference allele. For coelectroporation experiments with *MYB* small interfering RNA (siRNA), luciferase plasmids were cotransfected with Qiagen FlexiTube siRNA solution

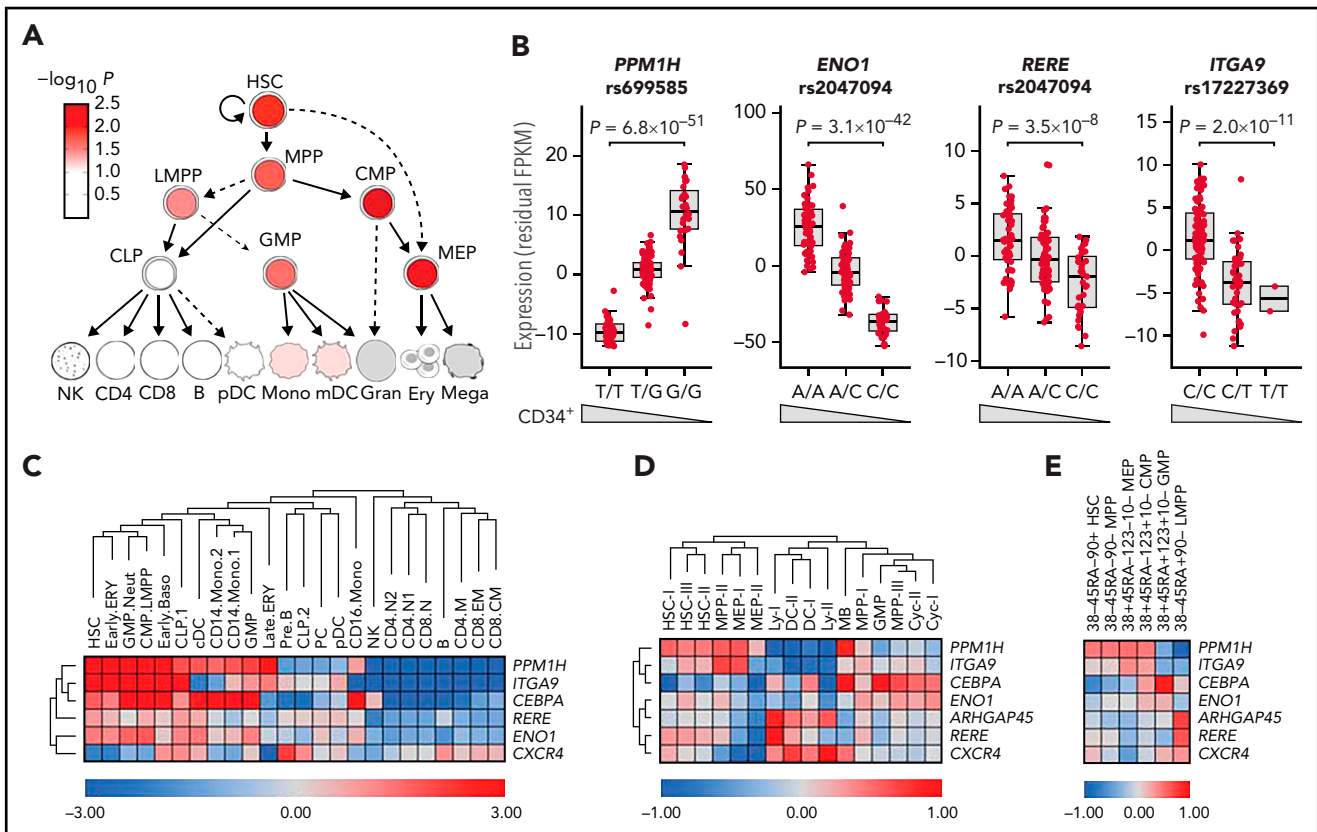


Figure 2. Effects on gene expression in HSPCs. (A) LD score regression shows enrichments of heritability in regions with accessible chromatin in HSPC subpopulations (red nuance indicates $-\log_{10} P$ value). (B) *cis*-eQTLs at *PPM1H*, *ENO1*, *RERE*, and *ITGA9* identified RNA-seq data for CD34⁺ cells from 155 blood donors (supplemental Table 10). Data are residual fragments per kilobase of transcript per million mapped reads (FPKM) values after correction for 10 expression principal components. Wedges indicate directions of effects on blood CD34⁺ cell levels for the same variant. (C) Candidate gene expression in single-cell messenger RNA-seq data from 35 582 blood and bone marrow mononuclear cells¹⁷ (supplemental Figures 9 and 10). *ARHGAP45* was not represented in this data set. (D-E) Average expression of candidate genes across different cell clusters in single-cell Cellular Indexing of Transcriptomes and Epitopes by Sequencing data for 4905 lineage-negative CD34⁺ cells from adult bone marrow.¹⁸ In panel D, the 4905 cells have been clustered according to RNA-seq pattern (supplemental Figure 11). In panel E, the cells were instead clustered by gating using the sequence counts for the tags derived from antibodies to the CD38, CD45RA, CD90, CD123, and CD10 cell surface markers, as indicated at the upper edge of the heatmap (supplemental Figure 12). B, B cells; Baso, basophil; CD4, CD4⁺ T cells; CD8, CD8⁺ T cells; CLP, common lymphoid progenitors; Cyc, cycling cells; DC, dendritic cells; ERY, erythroid progenitors; GMP, granulocyte-monocyte progenitors; LMPP, lymphoid-primed multipotent progenitors; Mono, monocyte; PC, plasma cells; PreB, pre-B cells; Neut, neutrophil; NK, natural killer cells.

targeting *MYB* or Qiagen Negative Control siRNA. Lysates for luciferase activity measurement and Western blot were collected simultaneously, 24 hours after electroporation. Knockdown was confirmed by western blot using a recombinant c-Myb antibody.

Motif analysis

For motif analysis, we used PERFECTOS-APE (<http://opera.autosome.ru/perfectosape>) with the HOCOMOCO-10, JASPAR, HT-SELEX, SwissRegulon, and HOMER motif databases.

shRNA-knockdown in umbilical cord blood cells

Umbilical cord blood samples were obtained from newborns at Skåne University Hospital (Lund and Malmö, Sweden) and Helsingborg Hospital (Helsingborg, Sweden), in compliance with regulations set by the regional ethical committee and informed consent. Mononuclear cells were isolated by density gradient centrifugation within 48 hours of sample collection and kept at -80°C . Thawed cord blood-derived CD34⁺ cells were sorted, lentivirally transduced with *PPM1H*-targeting or nontargeting (control) shRNA, and maintained in serum-free expansion medium supplemented with stem cell factor, thrombopoietin, and FMS-like tyrosine kinase 3 ligand. Using flow cytometry, the

percentages and absolute counts (using CountBright beads; Thermo Fisher Scientific) of CD34⁺ and CD34⁺90⁺ cells at days 7, 14, and 21 were measured. Cell enrichment was calculated by dividing CD34⁺ and CD34⁺90⁺ counts at each time point by initial cell counts, and then normalizing the enrichment values to the control shRNA-transduced cells at the same time point. At each time point, 3 transduction replicates were recorded. The experiment was repeated 3 times.

For statistical analysis, we compared normalized enrichment values at days 7, 14, and 21 for shRNA-transduced cells vs nontargeting shRNA control. To ensure a conservative analysis, we first averaged the transduction replicates for each experiment, then calculated *P* values using permutation testing with day 7, 14, and 21 data for the same experiment being permuted within each day stratum (100 000 permutations).

Results

Genome-wide association study

Blood CD34⁺ cell levels were analyzed in 13 167 blood donors and primary care patients from southern Sweden

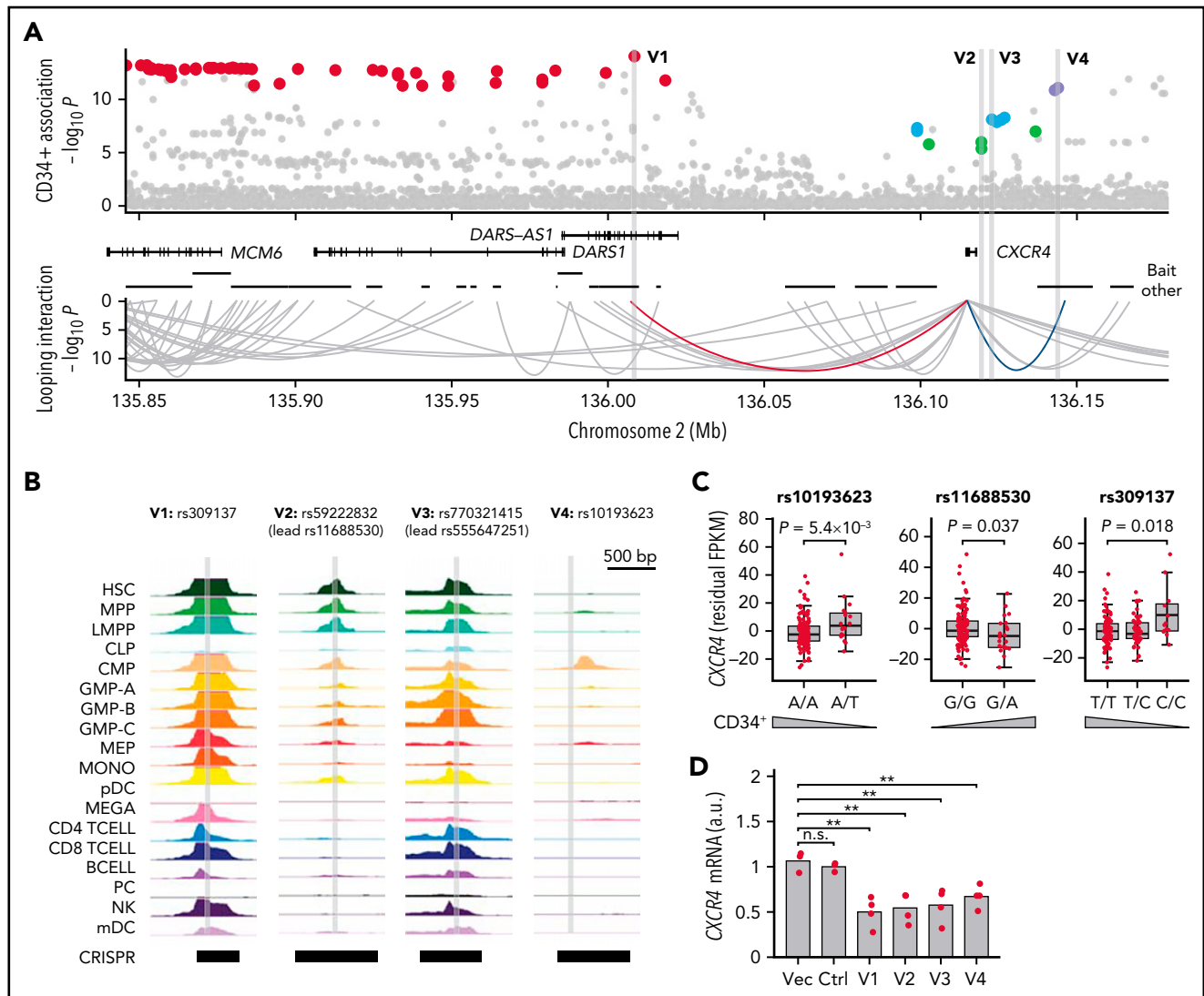


Figure 3. Associations with CXCR4. (A) Four independent associations were detected at 2q22. Credible sets (supplemental Table 9) indicated in red (lead variant rs309137), green (rs11688530), cyan (rs555647251), and blue (rs10193623). Using ATAC-seq and PCHI-C data, a single plausible causal variant was identified within each set. rs59222832 (“V2”; in credible set of rs11688530) and rs770321415 (“V3”; in credible set of rs555647251) map to the CXCR4 promoter region, 4.7 and 1.3 kb upstream of the transcription start site, respectively. In the other 2 credible sets, the lead variants rs309137 (“V1”) and rs10193623 (“V4”) were identified as likely causal based on looping interactions with the promoter (red and blue arches; y-axis indicates PCHI-C P-score). (B) Chromatin accessibility at putative causal variants in 18 blood cell types (y-axis indicates ATAC-seq signal): HSCs, MPPs, lymphoid-primed multipotent progenitors (LMPP), common lymphoid progenitors (CLP), common myeloid progenitors (CMP), granulocyte-monocyte progenitors (GMPs), MEPs, monocyte (MONO), megakaryocyte (MEGA), CD4⁺ T cells (CD4 TCELL), CD8⁺ T-cells (CD8 TCELL), B cells (BCELL), natural killer cells (NK), myeloid and plasmacytoid dendritic cells (mDC and pDC, respectively), and plasma cells (PC). (C) Conditional CXCR4 cis-eQTLs for the 3 common variants in our CD34⁺ cell RNA-seq data (n = 155). Wedges indicate directions of effects on blood CD34⁺ cell levels. Data are residual Fragments Per Kilobase of transcript per Million mapped reads (FPKM) values after correction for the 2 covariate lead variants and 10 principal components. P values for multivariable regression, one-sided in the direction opposite the effect on blood CD34⁺ cell levels of the illustrated variant. (D) CXCR4 expression in MOLM13 cells subjected to CRISPR/Cas9 editing with empty vector (Vec), a nontargeting sgRNA pair (Ctrl), or sgRNA pairs designed to delete 587 to 1421 bp regions harboring the 4 putative causal variants (3-4 biological replicates per condition) (supplemental Table 4; supplemental Figure 14). a.u., arbitrary units; mRNA, messenger RNA; n.s., not significant; **P < .01.

(aged 18-71 years) (Figure 1A; supplemental Table 1; supplemental Figure 1). In each sample, we analyzed up to 1 million white blood cells and defined the CD34⁺ cell level as the number of CD34⁺ cells divided by the number of CD45⁺ mononuclear cells (supplemental Tables 2 and 3; supplemental Figures 2 and 3). To assess reproducibility, 660 individuals were sampled twice, with 3 to 36 months between samplings; significant correlation was found between replicates (Spearman $P = 1.3 \times 10^{-84}$; $r^2 = 0.44$) (supplemental

Figure 4). Higher blood CD34⁺ cell levels were observed in male subjects than in female subjects (supplemental Figure 5), but no association with age was noted.

The participants were genotyped for 18 million variants by using SNP microarrays and imputation. For association analysis, the data were partitioned into a discovery set of 10 949 individuals of Swedish ancestry and a follow-up set of 2218 individuals of other European ancestry (supplemental Table 1; supplemental

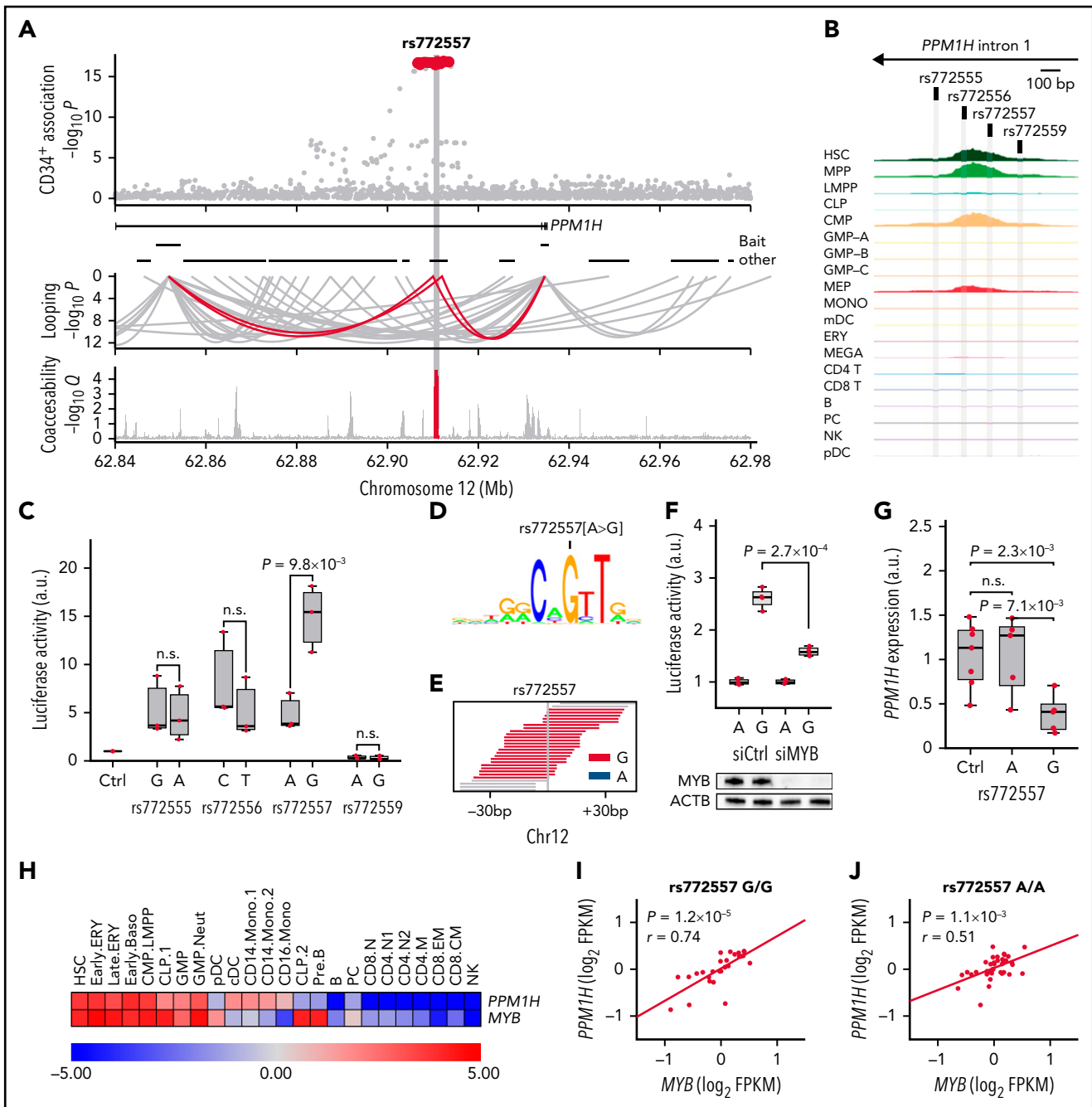


Figure 4. Association with PPM1H. (A) Top: close-up of the 12q14 signal. Middle: chromatin looping interactions in CD34⁺ cells with standard and internal promoter (red arches; y-axis indicates PCHI-C P -score). Bottom: positive correlation between PPM1H expression across sorted blood cell populations and ATAC-seq signal⁴⁵ (100 bp sliding window) in an ~500-bp-long chromosomal segment in intron 1 (red peak)⁴⁵ (y-axis indicates false discovery rate for Pearson correlation). (B) Four credible set variants (supplemental Table 9) map to the identified segment, which is accessible in HSCs, MPPs, CMPs, and MEPs (y-axis indicates ATAC-seq signal). (C) Luciferase activities of the 4 candidate causal variants in K562 cells (3 biological replicates). P values for one-sided Student t test in the *cis*-eQTL direction. Data normalized to empty vector control (Ctrl). (D) MYB motif logo; rs772557[A>G] alters a critical recognition base. (E) Chromatin immunoprecipitation with massively parallel DNA sequencing for MYB in Jurkat cells (rs772557-heterozygous) showing exclusive pull-down of rs772557-G reads. (F) siRNA knockdown of MYB in K562 cells attenuates rs772557-G luciferase activity (3-4 biological replicates). P value is for one-sided Student t test. (G) CRISPR/Cas9 disruption of rs772557 (supplemental Figure 16) in K562 cells (5 biological targeting replicates; 7 biological control replicates). P values are for one-sided Student t test. (H) Coexpression of PPM1H and MYB across blood cell types. Data are bulked single-cell messenger RNA-seq data from 35 582 blood and bone marrow mononuclear cells.¹⁷ (I-J) CD34⁺ cell RNA-seq data revealed stronger correlation between MYB and PPM1H expression in rs772557-G homozygotes ($n = 27$) than in rs772557-A homozygotes ($n = 37$). Data are \log_2 -transformed fragments per kilobase of transcript per million mapped reads (FPKM) values, median-centered per genotype group. P and r values are for Pearson correlation. a.u., arbitrary units; B, B cells; Baso, basophil; CD4, CD4⁺ T cells; CD8, CD8⁺ T cells; CLP, common lymphoid progenitors; Cyc, cycling cells; DC, dendritic cells; ERY, erythroid progenitors; GMP, granulocyte-monocyte progenitors; LMPP, lymphoid-primed multipotent progenitors; mDC, myeloid dendritic cells; Mono, monocyte; n.s., not significant; PC, plasma cells; pDC, plasmacytoid dendritic cells; PreB, pre-B cells; Neut, neutrophil; NK, natural killer cells.

Figures 6 and 7). To correct for multiple testing, variants were partitioned into 5 classes based on genomic annotations, and weighted Bonferroni adjustment was applied, taking into account the predicted functional impact of variants within each class (supplemental Methods).⁶

In a combined analysis of the 2 data sets, 6 association signals reached significance, and 2 were suggestive (within one order of magnitude from Bonferroni thresholds). Conditional analysis uncovered an additional 3 independent signals at the 2q22 locus, increasing the number of significant signals to 9 (Figure 1B), whereas no additional signals were detected at the other loci after accounting for their respective lead variants. No heterogeneity was detected in effect estimates between the discovery and follow-up data sets (Bonferroni-adjusted Cochran's Q P_{het} = not significant for all lead variants) (supplemental Table 5), nor between the different sample collection phases (Bonferroni-adjusted P_{het} = not significant for all lead variants) (supplemental Table 6); only the rare variant rs555647251 displayed significant heterogeneity between blood donors and primary care patients (Bonferroni-adjusted P_{het} = 0.046) (supplemental Table 7). The identified lead variants were polymorphic in all geographic ancestry super-populations in the 1000 Genomes Phase III compendium.²¹ The exception was rs555647251, which was only polymorphic in the European (EUR) and American (AMR) super-populations (supplemental Table 8). The proportion of variance explained by the lead variants of the 9 significant signals was 4.6% in the combined data set. Using LD score regression,¹² the total SNP heritability was estimated at 12.7%. We detected enrichments of heritability in chromatin regions accessible in HSPCs^{8,9} (Figure 2A), indicating that we preferentially identify variants that act by altering gene regulation intrinsically in these cell types.

Identification of candidate genes

To identify candidate genes based on HSPC-intrinsic effects, we generated expression quantitative trait locus (eQTL) data for sorted CD34⁺ cells from 155 blood donors using RNA-seq. In addition, we retrieved promoter capture Hi-C (PChI-C) data¹⁴ for CD34⁺ cells, and ATAC-seq data for sorted blood cells, including 7 HSPC populations.⁸

We defined the 99% credible sets of probable causal variants (supplemental Table 9) and prioritized genes as candidate genes if they: (1) had a non-synonymous coding variant within the credible set; (2) had a *cis*-eQTL in CD34⁺ cells (Figure 2B; supplemental Table 10); or (3) the credible set contained a regulatory variant in the promoter region, or in a region with a chromatin looping interaction with the promoter in CD34⁺ cells¹⁴ (supplemental Figure 8). As regulatory variants, variants in regions with accessible chromatin in HSPCs were considered.⁸ Strikingly, the identified candidate genes include both known HSPC-relevant genes (*CXCR4* and *CEBPA*) and genes never previously implicated in HSPC biology (*PPM1H*, *ENO1*, *RERE*, and *ARHGAP45*) or only minimally studied in this area (*ITGA9*)²² (Figure 1B).

Genetic overlap with human diseases and traits

To investigate further the impact of the identified variants, we questioned if these variants associate with other traits and diseases. Hence, we searched for coincident associations among variants in LD ($r^2 > 0.8$) with the lead variants in the UK Biobank

and the GWAS Catalog.²³⁻²⁷ We detected coincident associations with variants known to associate with mature blood cell traits (6 of the significant variants, at 2q22/*CXCR4*, 12q14/*PPM1H*, 1p36/*ENO1-RERE*, 19p13/*ARHGAP45*, 19q13/*CEBPA*), and hematologic malignancies and autoimmune disorders (variants at 2p22/*CXCR4* and 19p13/*CEBPA*) (supplemental Tables 11 and 12). Of note, 2 of the significant candidate genes underlie autosomal-dominant disorders defined by aberrant HSPC regulation: WHIM (warts, hypogammaglobulinemia, immunodeficiency and myelokathexis) syndrome (*CXCR4*)^{28,29} and familial acute myeloid leukemia (*CEBPA*).³⁰ Furthermore, somatic mutations in *CXCR4* and *CEBPA* have been reported in blood malignancies.³¹⁻³³

Gene expression in human hematopoiesis

We next explored the expression of the candidate genes across hematopoietic cell types. We observed enrichments of expression in HSPC vs non-HSPC populations, both in single-cell RNA-seq data for 35 582 mononuclear blood and bone marrow cells¹⁷ (one-sided Wilcoxon rank sum test, $P = 2.1 \times 10^{-10}$) (Figure 2C; supplemental Figure 9) and in bulk RNA-seq data⁸ (one-sided Wilcoxon rank-sum test, $P = 7.1 \times 10^{-5}$) (supplemental Figure 10).

To map expression within the CD34⁺ compartment, we used single-cell Cellular Indexing of Transcriptomes and Epitopes by Sequencing data for 4905 lineage-negative CD34⁺ bone marrow cells.¹⁸ This revealed distinct expression biases for the different candidate genes (Figure 2D-E; supplemental Figures 11 and 12; supplemental Table 13), including greater than fourfold enrichments in hematopoietic stem cells (HSCs), multi-potential progenitors (MPPs), megakaryocyte-erythrocyte progenitors (MEPs), and mast cell/basophil progenitors (MBs) for *PPM1H* (5.86- to 14.1-fold enrichment; one-sided Wilcoxon rank sum test, $P = 2.01 \times 10^{-4}$ to 1.35×10^{-11}); in HSC, MPP, and MEP populations for *ITGA9* (4.74- to 11.1-fold; $P = 1.98 \times 10^{-3}$ to 2.38×10^{-10}); in MB, dendritic cell, and lymphoid (Ly) precursors for *CXCR4* (4.00- to 9.79-fold; $P = 1.56 \times 10^{-18}$ to 6.17×10^{-67}); in Ly populations for *RERE* (4.28-fold; $P = 6.40 \times 10^{-7}$); and in MPP, MB, dendritic cell, Ly, and granulocyte-monocyte progenitor populations for *CEBPA* (4.38- to 24.3-fold; $P = 2.55 \times 10^{-3}$ to 2.32×10^{-80}). In addition, we observed greater than twofold enrichment of expression in MPPs for *ENO1* (2.18- to 2.23-fold; $P = 2.98 \times 10^{-95}$ to 1.25×10^{-101}) and in Ly for *ARHGAP45* (2.28- to 2.99-fold; $P = 4.96 \times 10^{-5}$ to 1.16×10^{-5}) (supplemental Table 13). These data further support that the identified candidate genes are relevant to HSPCs.

Associations with *CXCR4*

Four signals map to *CXCR4* (C-X-C chemokine receptor type 4) at 2q22. This receptor binds stromal-derived factor-1 (SDF-1; also known as CXCL12). Internalization of *CXCR4* is required for HSPC egression from the bone marrow.³⁴ In the WHIM syndrome, gain-of-function mutations in the C-terminal region prevent internalization after stimulation, leading to retention of HSPCs and other white blood cells in the bone marrow.³⁵ *CXCR4* inhibitors are one of the current methods for mobilizing CD34⁺ cells for leukapheresis.³⁶ The fact that we identify association with *CXCR4* provides proof-of-principle for our idea that regulators of blood CD34⁺ cell levels can be exposed in vivo in humans through genetic variation.

The *CXCR4* signals represent 3 common and 1 rare variant (Figure 1B). Within each of their credible sets (supplemental Table 9), we identified a single regulatory variant that either maps to, or has a looping interaction with, the *CXCR4* promoter, making them plausible causal variants (Figure 3A; supplemental Figure 8A). In the sets of rs11688530 and rs555647251, rs59222832 and rs770321415 were identified as regulatory promoter variants. In the other 2 sets, the lead variants rs309137 and rs10193623 were identified as likely causal based on looping interactions.

Because *CXCR4* is a known negative regulator of HSPC regression, we looked for effects of the identified variants on *CXCR4* expression in CD34⁺ cells in the direction opposite their effects on blood CD34⁺ cell levels. Indeed, multivariable analysis of our CD34⁺ cell RNA-seq data for blood donors unveiled conditional *CXCR4* cis-eQTLs for the 3 common variants (one-sided linear regression, $P = 5.4 \times 10^{-3}$ to 1.8×10^{-2}) (Figure 3B), although the rare variant rs555647251 was not polymorphic in this data set. Furthermore, using CRISPR/Cas9, we deleted the 4 putative causal variants in MOLM13 acute myeloid leukemia cells (supplemental Table 4; supplemental Figures 13 and 14), yielding *CXCR4* downregulation (Figure 3C). These data suggest that the 2q22 associations are caused by genetic variation in genomic regions required for *CXCR4* expression in HSPCs.

Association with *PPM1H*

Our most significant association maps to *PPM1H* (protein phosphatase, Mg²⁺/Mn²⁺ dependent 1H), encoding an evolutionarily conserved serine/threonine phosphatase.^{37,38} The few studies that have been performed suggest that *PPM1H* could be involved in cell signaling,³⁹⁻⁴¹ trastuzumab resistance,⁴² lupus,⁴³ and colon cancer.⁴⁴ Notably, our cis-eQTL analysis revealed an anticorrelation between *PPM1H* expression and CD34⁺ cell levels (Figure 2B).

The *PPM1H* credible set contains 32 variants in intron 1 (Figure 4A; supplemental Table 9). The associated region has looping interactions, both with the standard promoter and an internal promoter (Figure 4A; supplemental Figure 8B). By integrating ATAC- and RNA-seq data for sorted blood cell types,⁴⁵ a positive correlation was found between *PPM1H* expression and chromatin accessibility in an ~500-bp-long segment within the associated region (one-sided Pearson correlation, $P = 4.2 \times 10^{-9}$; false discovery rate = 2.5×10^{-5}) (Figure 4A). Consistent with the gene expression data analysis (Figure 2C-E), this segment is accessible in HSCs, MPPs, MEPs, and common myeloid progenitors (CMPs) (Figure 4B).

The identified segment overlaps 4 credible set variants (rs772555, rs772556, rs772557, and rs772559). For functional fine-mapping, we conducted luciferase experiments with constructs representing their reference and alternative alleles in K562 erythroleukemia cells. Significantly higher luciferase activity was observed with the rs772557-G construct than with the rs772557-A construct (one-sided Student *t* test, $P = 9.8 \times 10^{-3}$) (Figure 4C), consistent with the cis-eQTL direction (rs772557[A>G] is in LD with rs669585[T>G]; $r^2 = 0.98$). We also found higher accessibility at rs772557-G than at rs772557-A in DNase-sequencing data⁴⁶ for heterozygous adult CD34⁺ cells (125 vs 47 reads; binomial test, $P = 2.0 \times 10^{-8}$).

Motif analysis predicted that the rs772557-G allele contains an MYB transcription factor-binding site that is abrogated by the rs772557-A allele (Figure 4D; supplemental Table 14). Consistent with this finding, chromatin immunoprecipitation sequencing for MYB in Jurkat cells (heterozygous for rs772557) showed exclusive pull-down of rs772557-G (Figure 4E; supplemental Figure 15). In addition, luciferase experiments with cotransfected MYB siRNA showed selective attenuation of signal from rs772557-G construct but had no impact on signal from rs772557-A construct (one-sided Student *t* test, $P = 2.7 \times 10^{-4}$ for MYB siRNA-treated cells vs controls) (Figure 4F).

For further functional validation, we perturbed rs772557 by CRISPR/Cas9 in K562 cells, which are triploid-heterozygous for rs772557, having 2 copies of the rs772557-G allele and 1 copy of the rs772557-A allele. Serendipitously, we identified sgRNA sequences that overlap rs772557 and enable allele-specific disruption by cutting DNA only 1 bp upstream of rs772557 (supplemental Figure 16; supplemental Table 4). We observed *PPM1H* downregulation with rs772557-G sgRNA (one-sided Student *t* test, $P = 2.3 \times 10^{-3}$ for rs772557-G-sgRNA-treated vs sgRNA-control-treated cells; $P = 7.1 \times 10^{-3}$ for rs772557-G-sgRNA-treated vs rs772557-A-sgRNA-treated cells) (Figure 4G). In addition, *MYB* and *PPM1H* are coexpressed across blood cell types (Figure 4H), and, in our CD34⁺ cell RNA-seq data for blood donors, stronger positive correlation was observed between *MYB* and *PPM1H* expression among 27 rs772557-G homozygotes (Pearson correlation $r = 0.74$; $P = 1.2 \times 10^{-5}$) (Figure 4I) than among 37 rs772557-A homozygotes (Pearson correlation $r = 0.51$; $P = 1.1 \times 10^{-3}$) (Figure 4J), with a borderline-significant difference between the 2 correlation coefficients (one-sided Fisher *Z* test, $P = .08$). Consistent with an additive allele dose effect, an intermediate correlation was observed among 85 rs772557-A/G heterozygotes (Pearson correlation $r = 0.56$; $P = 2.3 \times 10^{-8}$). Finally, shRNA-knockdown of *PPM1H* in primary CD34⁺ umbilical cord blood cells resulted in higher proportions of CD34⁺ and CD34⁺90⁺ cells relative to control (supplemental Figures 17 and 18). These data identify rs772557 as a causal variant and further support a functional anticorrelation between *PPM1H* expression and blood CD34⁺ cell levels.

Additional associations

Among the remaining significant associations, 1p36/*ENO1-RERE* and 3p22/*ITGA9* exhibit cis-eQTLs in CD34⁺ cells (Figure 2B). *ENO1* encodes the glycolytic enzyme α -enolase 1; a shorter isoform binds the *MYC* promoter as a tumor suppressor.⁴⁷ *RERE* encodes a transcription factor that binds the retinoic acid receptor.⁴⁸ The credible set contains a candidate causal regulatory variant between *ENO1* and *RERE* that interacts with both promoters (supplemental Figure 8C; supplemental Table 9). *ITGA9* encodes integrin α -9, which is expressed in HSPCs,⁴⁹ but its role remains unclear. The identified association maps to *ITGA9* introns 3 and 4, with four regulatory variants in intron 3 looping to the promoter (supplemental Figure 8D; supplemental Table 9). Finally, the 19p13 signal tags a missense variant in *ARHGAP45*, encoding minor histocompatibility protein HA-1, a regulator of T- and B-cell migration.⁵⁰ Interestingly, recent mouse data suggest that *Arhgap45* also regulates HSPC engraftment in bone marrow.⁵¹

Among the suggestive associations, the 8q24 signal maps to *CCDC26*, but PCHi-C analysis revealed a long-distance looping interaction with the *MYC* promoter, 1.86 Mb away (supplemental Figure 8H). Interestingly, the identified signal corresponds to the Blood Enhancer Cluster (BENC), an evolutionarily conserved “super-enhancer” required for *Myc* expression in mouse HSPCs.⁵² The BENC comprises 8 enhancer modules (denoted A to H). Our signal spans module D. Deletion of this module in mice affects *Myc* expression in HSCs and MPPs. Finally, the second suggestive signal maps to *TERT*. Mutations in *TERT* cause dyskeratosis congenita, in which impaired telomere maintenance leads to problems with HSPC regeneration and increased risk of myelodysplastic syndrome.⁵³ Somatic mutations in *TERT* and *MYC* have also been reported in blood malignancies.³³

Discussion

We report the first large-scale GWAS on blood CD34⁺ cell levels. We identify 9 significant association signals explaining approximately one-third of the total estimated SNP heritability (4.6% of 12.7%). This study represents the first successful GWAS on a stem cell trait, and the results provide proof-of-principle for the idea that HSPC regulators can be identified in vivo in humans through genetic variation.

We identified associations with known regulators of blood CD34⁺ cell levels, as well as with 5 novel regulators (*PPM1H*, *ENO1*, *RERE*, *ITGA9*, and *ARHGAP45*). Understanding the mechanisms and molecular pathways that underlie these associations poses intriguing challenges. The clinical efficacy of CXCR4 antagonists in the context of stem cell mobilization, and our data (Figure 3), suggest that the rate of egression of CD34⁺ cells is the key variable in the case of the CXCR4 associations. At the same time, variation in blood CD34⁺ cell levels can reflect variation in several physiological variables, including egression rate, time spent in the bloodstream, and stem cell pool size. Potentially, the identified variants and genes could affect either, or several, of these variables.

Today, the most common method to harvest stem cells for transplantation is by leukapheresis, requiring mobilization of HSPCs into the blood. Current mobilization regimens include cyclophosphamide, granulocyte colony-stimulating factor, and CXCR4 inhibitors. Intriguingly, for the most significant locus, we discovered an anticorrelation between *PPM1H* expression and CD34⁺ levels, supported by *cis*-eQTL, functional fine-mapping, and shRNA-knockdown data (Figures 2B and 4). This finding suggests that *PPM1H* could be used as an inhibition target to facilitate stem cell harvesting by leukapheresis, although further studies are needed to understand the biology of *PPM1H* and to identify pharmacologic inhibitors. Regarding potential side effects of such inhibitors, *PPM1H* has not been associated with any severe disease according to GWAS Catalog and UK Biobank data.^{27,54} Although the gene is conserved against loss-of-function variants relative to synonymous coding variants (observed/expected score 0.18 vs 0.98 in the Genome Aggregation Database, gnomAD⁵⁵), the UK Biobank database contains 32 individuals with loss-of-function *PPM1H* variants (<https://www.ukbiobank.ac.uk> and <https://azphewas.com>), all of whom were aged >40 years at recruitment, with >10 years of follow-up.²⁶ Moreover, the effects of any inhibitor, when used in the context of stem cell mobilization, will likely be short term. Other notable findings include *ENO1* as a regulatory enzyme with links to the

MYC pathway, *RERE* as a transcription factor with links to retinoic acid signaling, and *ITGA9* as a cell surface marker with a functional role in the regulation of blood CD34⁺ cell levels. In all, we report the first large-scale analysis of the genetic architecture of blood CD34⁺ cell levels, with potential implications for stem cell harvesting and transplantation.

Acknowledgments

The authors are indebted to Ellinor Jonsson and the personnel at the Clinical Chemistry and Clinical Immunology and Transfusion Medicine in Region Skåne for their assistance, and the patients and blood donors who participated in the study.

This work was supported by grants from the European Research Council (CoG-770992), the Knut and Alice Wallenberg Foundation (2014.0071 and 2017.0436), the Swedish Research Council (2017-02023 and 2018-00424), the Swedish Cancer Society (2017/265 and 20.0694), the Swedish Children’s Cancer Fund (PR2018-0118 and TJ2017-0042), and the Inga Britt & Arne Lundberg Research Foundation (2017-0055).

Authorship

Contribution: A.L.d.L.P., U.T., J.L., K.S., and B.N. conceived the study; A.L.d.L.P., L.E., C.C., Z.A., M.P., K.Ž., G.N., U.T., J.L., K.S., and B.N. designed experiments; A.L.d.L.P., C.C., and N.M. developed flow cytometry protocols; L.E. and A.L.A. developed AliGater; A.L.d.L.P., L.E., C.C., Z.A., N.M., N.U.D., and D.B. performed the phenotyping; A.L.d.L.P., C.C., G.T., M.P., U.T., and K.S. performed genetic analyses; C.C., Z.A., N.M., and K.Ž. conducted functional experiments; A.L.d.L.P., L.E., C.C., Z.A., N.M., G.T., K.Ž., A.L.A., M.T., M.P., P.D., E.B., A.N., V.G.S., G.K., and B.N. performed data analyses; and A.L.d.L.P., L.E., C.C., Z.A., and B.N. drafted the manuscript. All authors contributed to the final manuscript.

Conflict-of-interest disclosure: G.T., G.N., U.T., and K.S. are employed by deCODE genetics/Amgen Inc. V.G.S. serves as an advisor to and/or has equity in Branch Biosciences, Ensoma, Novartis, Forma, and Cellarity, all unrelated to this work. The remaining authors declare no competing financial interests.

ORCID profiles: L.E., 0000-0002-4257-7284; K.Ž., 0000-0002-4098-0184; M.T., 0000-0001-6244-3841; P.D., 0000-0002-8070-7238; D.B., 0000-0003-3178-1586; N.U.D., 0000-0003-4938-3973; V.G.S., 0000-0003-0044-443X.

Correspondence: Björn Nilsson, Hematology and Transfusion Medicine, Department of Laboratory Medicine, BMC B13, 221 84 Lund, Sweden; e-mail: bjorn.nilsson@med.lu.se.

Footnotes

Submitted 6 July 2021; accepted 11 December 2021; prepublished online on *Blood* First Edition 10 January 2022. DOI 10.1182/blood.2021013220.

*L.E., C.C., and Z.A. contributed equally to this study and are joint second authors.

The sequencing data and counts of fragments per kilobase of transcript per million mapped reads are available from the European Genome Archive repository (accession numbers EGAS00001005655 and EGAD00001008194).

The online version of this article contains a data supplement.

The publication costs of this article were defrayed in part by page charge payment. Therefore, and solely to indicate this fact, this article is hereby marked “advertisement” in accordance with 18 USC section 1734.

REFERENCES

- Notta F, Zandi S, Takayama N, et al. Distinct routes of lineage development reshape the human blood hierarchy across ontogeny. *Science*. 2016;351(6269):aab2116.
- Barnett D, Janossy G, Lubenko A, Matutes E, Newland A, Reilly JT; General Haematology Task Force of the British Committee for Standards in Haematology. Guideline for the flow cytometric enumeration of CD34+ haematopoietic stem cells. Prepared by the CD34+ Haematopoietic Stem Cell Working Party. *Clin Lab Haematol*. 1999;21(5):301-308.
- Cohen KS, Cheng S, Larson MG, et al. Circulating CD34(+) progenitor cell frequency is associated with clinical and genetic factors. *Blood*. 2013;121(8):e50-e56.
- Eidenschink L, Dizerega G, Rodgers K, et al. Basal levels of CD34 positive cells in peripheral blood differ between individuals and are stable for 18 months. *Cytometry B Clin Cytom*. 2012;82(1):18-25.
- Mantel N, Haenszel W. Statistical aspects of the analysis of data from retrospective studies of disease. *J Natl Cancer Inst*. 1959; 22(4):719-748.
- Sveinbjornsson G, Albrechtsen A, Zink F, et al. Weighting sequence variants based on their annotation increases power of whole-genome association studies. *Nat Genet*. 2016;48(3):314-317.
- Maller JB, McVean G, Byrnes J, et al; Wellcome Trust Case Control Consortium. Bayesian refinement of association signals for 14 loci in 3 common diseases. *Nat Genet*. 2012;44(12):1294-1301.
- Ulirsch JC, Lareau CA, Bao EL, et al. Interrogation of human hematopoiesis at single-cell and single-variant resolution. *Nat Genet*. 2019;51(4):683-693.
- Corces MR, Buenrostro JD, Wu B, et al. Lineage-specific and single-cell chromatin accessibility charts human hematopoiesis and leukemia evolution. *Nat Genet*. 2016; 48(10):1193-1203.
- Buenrostro JD, Wu B, Chang HY, Greenleaf WJ. ATAC-seq: a method for assaying chromatin accessibility genome-wide. *Curr Protoc Mol Biol*. 2015;109:21.29.1-21.29.9.
- Meuleman W, Muratov A, Rynes E, et al. Index and biological spectrum of human DNase I hypersensitive sites. *Nature*. 2020; 584(7820):244-251.
- Bulik-Sullivan BK, Loh PR, Finucane HK, et al; Schizophrenia Working Group of the Psychiatric Genomics Consortium. LD score regression distinguishes confounding from polygenicity in genome-wide association studies. *Nat Genet*. 2015;47(3):291-295.
- Finucane HK, Bulik-Sullivan B, Gusev A, et al; RACI Consortium. Partitioning heritability by functional annotation using genome-wide association summary statistics. *Nat Genet*. 2015;47(11):1228-1235.
- Mifsud B, Tavares-Cadete F, Young AN, et al. Mapping long-range promoter contacts in human cells with high-resolution capture Hi-C. *Nat Genet*. 2015;47(6):598-606.
- Mansour MR, Abraham BJ, Anders L, et al. Oncogene regulation. An oncogenic super-enhancer formed through somatic mutation of a noncoding intergenic element. *Science*. 2014;346(6215):1373-1377.
- Gioia L, Siddique A, Head SR, Salomon DR, Su AI. A genome-wide survey of mutations in the Jurkat cell line. *BMC Genomics*. 2018;19(1):334.
- Granja JM, Klemm S, McGinnis LM, et al. Single-cell multiomic analysis identifies regulatory programs in mixed-phenotype acute leukemia. *Nat Biotechnol*. 2019;37(12): 1458-1465.
- Sommarin MNE, Dhapola P, Safi F, et al. Single-cell multiomics reveals distinct cell states at the top of human hematopoietic hierarchy. *bioRxiv*. Preprint posted online 2 April 2021. doi: <https://doi.org/10.1101/2021.04.01.437998>.
- Becht E, McInnes L, Healy J, et al. Dimensionality reduction for visualizing single-cell data using UMAP. *Nat Biotechnol*. 2018;37(1):38-47.
- van Dijk D, Sharma R, Nainys J, et al. Recovering gene interactions from single-cell data using data diffusion. *Cell*. 2018; 174(3):716-729.e27.
- Auton A, Brooks LD, Durbin RM, et al; 1000 Genomes Project Consortium. A global reference for human genetic variation. *Nature*. 2015;526(7571):68-74.
- Schreiber TD, Stein C, Essl M, et al. The integrin $\alpha 9 \beta 1$ on hematopoietic stem and progenitor cells: involvement in cell adhesion, proliferation and differentiation. *Haematologica*. 2009;94(11):1493-1501.
- Staley JR, Blackshaw J, Kamat MA, et al. PhenoScanner: a database of human genotype-phenotype associations. *Bioinformatics*. 2016;32(20):3207-3209.
- Kamat MA, Blackshaw JA, Young R, et al. PhenoScanner V2: an expanded tool for searching human genotype-phenotype associations. *Bioinformatics*. 2019;35(22):4851-4853.
- Machiela MJ, Chanock SJ. LDlink: a web-based application for exploring population-specific haplotype structure and linking correlated alleles of possible functional variants. *Bioinformatics*. 2015;31(21):3555-3557.
- Bycroft C, Freeman C, Petkova D, et al. The UK Biobank resource with deep phenotyping and genomic data. *Nature*. 2018;562(7726): 203-209.
- Buniello A, MacArthur JAL, Cerezo M, et al. The NHGRI-EBI GWAS Catalog of published genome-wide association studies, targeted arrays and summary statistics 2019. *Nucleic Acids Res*. 2019;47(D1):D1005-D1012.
- Milanesi S, Locati M, Borroni EM. Aberrant CXCR4 signaling at crossroad of WHIM syndrome and Waldenström's macroglobulinemia. *Int J Mol Sci*. 2020; 21(16):1-15.
- Heusinkveld LE, Majumdar S, Gao JL, McDermott DH, Murphy PM. WHIM syndrome: from pathogenesis towards personalized medicine and cure. *J Clin Immunol*. 2019;39(6):532-556.
- Smith ML, Cavenagh JD, Lister TA, Fitzgibbon J. Mutation of CEBPA in familial acute myeloid leukemia. *N Engl J Med*. 2004;351(23):2403-2407.
- Kaiser LM, Hunter ZR, Treon SP, Buske C. CXCR4 in Waldenström's macroglobulinemia: chances and challenges. *Leukemia*. 2021;35(2):333-345.
- Panuzzo C, Signorino E, Calabrese C, et al. Landscape of tumor suppressor mutations in acute myeloid leukemia. *J Clin Med*. 2020; 9(3):802.
- Mitelman F, Johansson B and Mertens F (Eds.) Mitelman Database of Chromosome Aberrations and Gene Fusions in Cancer (2022). <https://mitelmandatabase.isb-cgc.org>.
- Karpova D, Bonig H. Concise review: CXCR4/CXCL12 signaling in immature hematopoiesis—lessons from pharmacological and genetic models. *Stem Cells*. 2015;33(8):2391-2399.
- Hernandez PA, Gorlin RJ, Lukens JN, et al. Mutations in the chemokine receptor gene CXCR4 are associated with WHIM syndrome, a combined immunodeficiency disease. *Nat Genet*. 2003;34(1):70-74.
- Liles WC, Broxmeyer HE, Rodger E, et al. Mobilization of hematopoietic progenitor cells in healthy volunteers by AMD3100, a CXCR4 antagonist. *Blood*. 2003;102(8): 2728-2730.
- Madeira F, Park YM, Lee J, et al. The EMBL-EBI search and sequence analysis tools APIs in 2019. *Nucleic Acids Res*. 2019;47(W1): W636-W641.
- Toft N, Birgens H, Abrahamsson J, et al. Results of NOPHO ALL2008 treatment for patients aged 1-45 years with acute lymphoblastic leukemia. *Leukemia*. 2018;32(3): 606-615.
- Sugiura T, Noguchi Y. Substrate-dependent metal preference of PPM1H, a cancer-associated protein phosphatase 2C: comparison with other family members. *Biomaterials*. 2009;22(3):469-477.
- Chen MJ, Dixon JE, Manning G. Genomics and evolution of protein phosphatases. *Sci Signal*. 2017;10(474):eaag1796.
- Berndsen K, Lis P, Yeshaw WM, et al. PPM1H phosphatase counteracts LRRK2 signaling by selectively dephosphorylating Rab proteins. *eLife*. 2019;8:1-37.
- Lee-Hoeflich ST, Pham TQ, Dowbenko D, et al. PPM1H is a p27 phosphatase implicated in trastuzumab resistance. *Cancer Discov*. 2011;1(4):326-337.
- Ghodke-Puranik Y, Imgruet M, Dorschner JM, et al. Novel genetic associations with interferon in systemic lupus erythematosus identified by replication and fine-mapping of trait-stratified genome-wide screen. *Cytokine*. 2020;132:154631.
- Sugiura T, Noguchi Y, Sakurai K, Hattori C. Protein phosphatase 1H, overexpressed in

- colon adenocarcinoma, is associated with CSE1L. *Cancer Biol Ther*. 2008;7(2):285-292.
45. Ulirsch JC, Nandakumar SK, Wang L, et al. Systematic functional dissection of common genetic variation affecting red blood cell traits. *Cell*. 2016;165(6):1530-1545.
46. Davis CA, Hitz BC, Sloan CA, et al. The Encyclopedia of DNA elements (ENCODE): data portal update. *Nucleic Acids Res*. 2018;46(D1):D794-D801.
47. Ghosh AK, Steele R, Ray RB. Functional domains of c-myc promoter binding protein 1 involved in transcriptional repression and cell growth regulation. *Mol Cell Biol*. 1999;19(4):2880-2886.
48. Vilhais-Neto GC, Maruhashi M, Smith KT, et al. Rere controls retinoic acid signalling and somite bilateral symmetry. *Nature*. 2010;463(7283):953-957.
49. Peng Y, Wu D, Li F, Zhang P, Feng Y, He A. Identification of key biomarkers associated with cell adhesion in multiple myeloma by integrated bioinformatics analysis. *Cancer Cell Int*. 2020;20(1):262.
50. Bleakley M, Riddell SR. Exploiting T cells specific for human minor histocompatibility antigens for therapy of leukemia. *Immunol Cell Biol*. 2011;89(3):396-407.
51. He L, Valignat M-P, Zhang L, et al. ARHGAP45 controls naïve T- and B-cell entry into lymph nodes and T-cell progenitor thymus seeding. *EMBO Rep*. 2021;22(4):e52196.
52. Bahr C, von Paleske L, Uslu VV, et al. A Myc enhancer cluster regulates normal and leukaemic haematopoietic stem cell hierarchies [published correction appears in *Nature*. 2018;558(7711):E4]. *Nature*. 2018;553(7689):515-520.
53. Vulliamy T, Marrone A, Goldman F, et al. The RNA component of telomerase is mutated in autosomal dominant dyskeratosis congenita. *Nature*. 2001;413(6854):432-435.
54. Karczewski KJ, Francioli LC, Tiao G, et al; Genome Aggregation Database Consortium. The mutational constraint spectrum quantified from variation in 141,456 humans [published correction appears in *Nature*. 2021;590(7846):E53]. *Nature*. 2020;581(7809):434-443.
55. Wang Q, Dhindsa RS, Carss K, et al; AstraZeneca Genomics Initiative. Rare variant contribution to human disease in 281,104 UK Biobank exomes. *Nature*. 2021;597(7877):527-532.

© 2022 by The American Society of Hematology